A Letters Journal Exploring the Frontiers of Physics

September 2015

EPL, **111** (2015) 50007
doi: 10.1209/0295-5075/111/50007

www.epljournal.org

Optimal synchronization of oscillatory chemical reactions with complex pulse, square, and smooth waveforms signals maximizes Tsallis entropy

Hisa-Aki Tanaka[1], Isao Nishikawa[1], Jürgen Kurths[2], Yifei Chen[3] and István Z. Kiss[3]

[1] *The University of Electro-Communications - Tokyo 182-8585, Japan*
[2] *The Potsdam Institute for Climate Impact Research - Telegraphenberg A31, 14473 Potsdam, Germany*
[3] *Department of Chemistry, Saint Louis University - St. Louis, MO 63103, USA*

received 1 June 2015; accepted in final form 24 August 2015
published online 18 September 2015

PACS 05.45.Xt – Synchronization; coupled oscillators
PACS 05.45.-a – Nonlinear dynamics and chaos
PACS 84.35.+i – Neural networks

Abstract – We show that the mathematical structure of Tsallis entropy underlies an important and ubiquitous problem in nonlinear science related to an efficient synchronization of weakly forced nonlinear oscillators. The maximization of the locking range of oscillators with the use of phase models is analyzed with general constraints that encompass forcing waveform power, magnitude, or area. The optimization problem is then recasted as a general form of Tsallis entropy maximization. The solution of these optimization problems is shown to be a direct consequence from Hölder's inequality. The resulting new maximization principle is confirmed in numerical simulations and experiments with chemical oscillations with nickel electrodissolution. While weakly nonlinear oscillators have generic optimal waveforms (sinusoidal, 50% duty cycle square wave, and equally paced bipolar pulses for power-, area-, and magnitude-constraints, respectively), strongly nonlinear oscillators require more complex waveforms such as smooth, square, and pulse ones.

Introduction. – Synchronization (injection locking) of oscillators to an external forcing (injection signal) of widely different waveforms is often used to provide means to timing of essential system processes. In many branches of science and engineering, methods for efficient synchronization have been developed in recent years, because the entrainment process plays a prominent role in the functioning of dynamical systems [1–3]. Different fields often use different waveforms: phase locking in nerve membrane dynamics with a sinusoidal current [4,5], circadian synchronization with light-dark cycles of a square waveform [3,6], and reset of the timing in pacemakers and electrical devices with pulse signals [7,8].

The various forcing waveforms called for establishing a theory for optimal synchronization of weakly forced nonlinear oscillators; phase-model–based theories proved to be useful because of their effectiveness in describing the synchronization process as well as their analytical tractability [1,2,9–11]. The shape of the forcing waveform profoundly impacts the efficiency of synchronization for applications requiring low-power consumptions. The width of the locking region requires waveforms related to a phase response curve (which shows the phase shift in the oscillations due to an instantaneous pulse signal) [1]. Fast synchronization [2], or desynchronization [9] is related to the derivative of the phase response curve. Different forcing techniques using square or pulse injection signals were developed for examples where the magnitude and the area of the signals were minimized [3,6,7]. Most previous theories resorted to variational calculus, such as the Euler-Lagrange equation, which are intended inherently for local optimization and limited to smooth signals [1,2,9]. In contrast, recent progresses [10,11] have shown that the optimal-synchronization problem for minimum power, magnitude, and area signals can be solved for a global optimization even with non-smooth signals, by means of Hölder's inequality [12]:

$$\|fg\|_1 \leq \|f\|_\alpha \|g\|_\beta, \tag{1}$$

in which $\|f\|_\alpha \equiv \langle |f(\theta)|^\alpha \rangle^{\frac{1}{\alpha}}$ denotes $[\int |f(\theta)|^\alpha \mathrm{d}\theta]^{\frac{1}{\alpha}}$, and $1 \leq \alpha, \beta \leq \infty$ and $\alpha^{-1} + \beta^{-1} = 1$. $\|f\|_\alpha$ amounts to the

L^α-norm of the function f if $\alpha > 0$. For this inequality, the following reverse form also holds (*i.e.*, the reverse Hölder's inequality):

$$\|fg\|_1 \geq \|f\|_\alpha \|g\|_\beta, \tag{2}$$

where $0 < \alpha < 1$ and $\alpha^{-1} + \beta^{-1} = 1$. Note that eq. (2) is directly obtained by setting $\| |fg|^{\frac{1}{\alpha}} |g|^{-\frac{1}{\alpha}} \|_1$ to the l.h.s. of Hölder's inequality (1) [12]. In eqs. (1), (2), $\|fg\|_1 = \|f\|_\alpha \|g\|_\beta$ holds if and only if there exist constants A and B, not both 0, such that $A|f(\theta)|^\alpha = B|g(\theta)|^\beta$ for almost all θ [12], which is referred to as the *equality condition*.

The general solution of the optimal synchronization implies that there might be a general mechanism that underlies the seemingly very different optimization problems (for power-, magnitude-, or area-constraints, respectively). In fact, entropy-based quantities often reflect the presence of a maximization mechanism under given constraints. Tsallis entropy [13,14] is one of such instances, which was proposed as a versatile framework for expansion of the realm of classical (Boltzmann-Gibbs) entropies for nonlinear processes, in particular, those that exhibit power-law behavior.

In this letter, as illustrated in fig. 1, we show that the mathematical structure of Tsallis entropy underlies an important and ubiquitous problem in nonlinear science related to an efficient synchronization of weakly forced nonlinear oscillators. We formulate a unified theoretical framework for optimal synchronization and Tsallis entropy maximization, *i.e.*, a new maximization principle. A general analysis of this maximization solution is performed for the characterization of optimal forcing signals for power-, magnitude-, and area-constraints. The theory is tested with numerical modeling of an electrochemical oscillatory process. Finally, we demonstrate the efficiency of smooth, square, and pulse signals obtained with the theory for establishing optimal synchronization (with power-, magnitude-, and area-constraints, respectively) in laboratory experiments with oscillatory nickel dissolution in sulfuric acid.

Tsallis entropy maximization underlies optimal synchronization. – In order to make the essence of our finding more transparent, we focus on the case of a single oscillator with one external weak forcing; however, the results can be extended for designing optimal $m : n$ mutual synchronization [11] in networks of weakly coupled nonlinear oscillators. We consider a general class of periodic functions $f(\theta)$ as the weak forcing, namely, those satisfying the following constraint: $||f||_r = M$, in which both r and M are positive constants. Especially for $r = 1, 2, \infty$, this constraint respectively defines the area-, power-, and magnitude-reduced forcings for a certain small M. Besides $\|f\|_r = M$, another constraint $\frac{1}{2\pi}\int_{-\pi}^{\pi} f(\theta)\mathrm{d}\theta = 0$, *i.e.*, a charge-balance constraint [1,2,15], is introduced, because total injection (injected charge) is required to be 0 in practical situations.

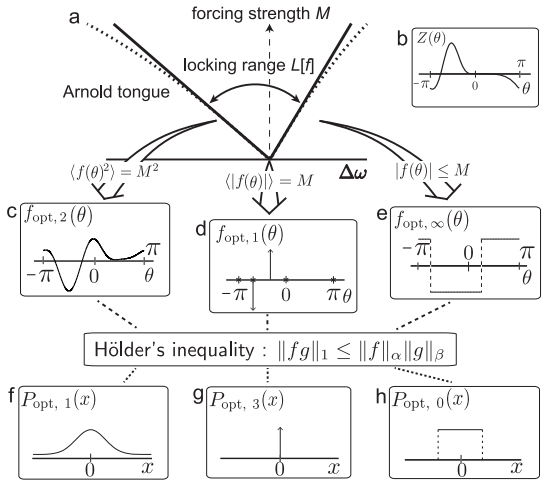

Fig. 1: Optimal forcings $f_{\mathrm{opt},\,r}$ maximizing synchronizability, and the associated escort functions $P_{\mathrm{opt},\,q}$ maximizing Tsallis entropy. (a) Arnold tongue determining the locking range. $\Delta\omega$ denotes the frequency difference between the oscillator and the forcing. (b) Phase response function Z for the Hodgkin-Huxley neuron model [2]. (c), (d), (e): curves represent the optimal forcings for $r = 2, 1, \infty$, respectively. (c) Power-reduced forcing, (d) area-reduced forcing, (e) magnitude-reduced forcing for the Hodgkin-Huxley neuron model [2]. (f), (g), (h): escort functions $P_{\mathrm{opt},\,q}(x)$ of probability distributions maximizing Tsallis entropy for $q = 1, 3, 0$, respectively. Note that for $q = 1$ Tsallis entropy is identified with the Boltzmann-Gibbs (BG) entropy since it converges to the BG entropy as $q \to 1 + 0$ [13].

Phase locking with a weak forcing $f(\theta)$ occurs when the slowly evolving phase difference ϕ between the oscillator and the forcing exhibits a stationary state, *i.e.*,

$$\mathrm{d}\phi/\mathrm{d}t = \Delta\omega + \Gamma(\phi) = 0, \tag{3}$$

where $\Delta\omega = \omega - \Omega$ is the difference between the forcing frequency Ω and the natural frequency ω of the oscillations, and $\Gamma(\phi)$ is a periodic function defined by $\Gamma(\phi) \equiv \frac{1}{2\pi}\int_{-\pi}^{\pi} Z(\theta+\phi) f(\theta)\mathrm{d}\theta$ and $Z(\theta)$ is the phase response (sensitivity) function (PRF) [16], obtained numerically or experimentally [17,18]. Note that this PRF is the same notion as the phase response curve (PRC) under weak inputs. The range of the frequency difference $\Delta\omega$ between the oscillator and the forcing, in which the solution for a stable steady state exists for ϕ, defines the locking range (synchronizability) $L[f(\theta)]$ for a certain fixed forcing waveform $f(\theta)$. For maximizing $L[f]$ under the constraint $\frac{1}{2\pi}\langle f(\theta)\rangle = 0$, the functional $J[f(\theta)] \equiv L[f] + \frac{\mu}{2\pi}\langle f(\theta)\rangle$ is introduced, where μ is a Lagrange multiplier and $\langle\cdot\rangle = \int_{-\pi}^{\pi} \cdot\, \mathrm{d}\theta$ [1]. Moreover, $J[f]$ is rewritten as the following inner product of f and g:

$$J[f(\theta)] = \frac{1}{2\pi}\langle f(\theta) g(\theta)\rangle, \tag{4}$$

where

$$g(\theta) = Z(\theta + \Delta\phi) - Z(\theta) + \mu. \tag{5}$$

μ and $\Delta\phi$ in eq. (5) are determined from Γ and the constraint on $\|f\|_r = M$, as shown later. It should also be noted that with the optimal waveform, $\Delta\phi$ becomes the difference between phase values of the maximum and minimum of $\Gamma(\phi)$. Thus, the optimal synchronizability can be defined by the following problem:

$$\text{maximize } J[f], \quad \text{subject to } \|f\|_r = M. \tag{6}$$

This optimal synchronization problem was previously solved by using the calculus of variations, only for $r = 2$ [1,2]. In addition to the case of $r = 2$, this problem was recently solved for general r, *i.e.*, for $1 \le r \le \infty$, via Hölder's inequality [10,11]. This finding hints at a new, complete analysis of Tsallis entropy maximization. Tsallis entropy is defined by the functional $S[p(x)]$ of the probability density function (PDF) $p(x)$,

$$S[p(x)] \equiv [1 - \langle p(x)^q \rangle_x]/(q-1), \tag{7}$$

where $\langle\cdot\rangle_x = \int_{-\infty}^{\infty} \cdot \, \mathrm{d}x$ [13]. In addition, the escort function of $p(x)$ is also defined as $P(x) \equiv p(x)^q / \langle p(x)^q \rangle_x$. For the parameter q, we usually assume $0 < q < 3$ and $q \neq 1$. Tsallis entropy maximization is then defined as

$$\begin{aligned} &\text{maximize } S[p(x)], \\ &\text{subject to } \langle p(x) \rangle_x = 1 \text{ and } \langle h(x) P(x) \rangle_x = \sigma^2, \end{aligned} \tag{8}$$

where we assume $h(x) = x^2$ which constrains the second moment of $P(x)$ to be σ^2.

Note for a given q and σ, eq. (8) is equivalent to the minimization of $\langle p(x)^q \rangle_x$ under the constraint $\langle (h(x) - \sigma^2) p^q(x) \rangle_x = 0$, *i.e.*, $\langle h(x) P(x) \rangle_x = \sigma^2$ in eq. (8). Therefore, by introducing the following functional $T[p(x)]$ and the multiplier λ, Tsallis entropy maximization is recast as the equivalent optimization:

$$\begin{aligned} &\text{minimize (or maximize)} \\ &T[p(x)] \equiv \sigma^2 \langle p(x)^q \rangle_x + \lambda \langle (h(x) - \sigma^2) p(x)^q \rangle_x \\ &\qquad = \langle p(x)^q [\lambda h(x) + (1-\lambda)\sigma^2] \rangle_x \\ &\text{for } q > 1 \text{ (or } q < 1), \quad \text{subject to } \langle p(x) \rangle_x = 1. \end{aligned} \tag{9}$$

This $T[p]$ of eq. (9) is directly mapped to Hölder's inequality in eq. (1) or eq. (2) by inserting

$$p(x)^q = f \text{ and } \lambda h(x) + (1-\lambda)\sigma^2 = g, \tag{10}$$

to $T[p]$. Namely, Tsallis entropy maximization is equivalent to the optimization:

$$\begin{aligned} &\text{maximize (or minimize) } \langle fg \rangle \text{ for } q < 1 \text{ (or } q > 1), \\ &\text{subject to } \|f\|_{\frac{1}{q}} = 1, \end{aligned} \tag{11}$$

in which $\langle fg \rangle = \langle p(x)^q [\lambda h(x) + (1-\lambda)\sigma^2] \rangle_x$ and $\|f\|_{\frac{1}{q}} = \|p^q\|_{\frac{1}{q}} = \langle p(x) \rangle_x = 1$. From eqs. (4), (6) and eq. (11), we realize that the mathematical structure of Tsallis entropy maximization underlies the optimal synchronization. We note that Rényi entropy maximization [13] is recast into the same form of eq. (11) if the constraints in eq. (8) are imposed, for instance.

Optimization with Hölder's inequality. – The features of the solution of the optimization problem (6) (or (11)) are now directly answered by Hölder's inequality. Below, we outline the resulting solutions to both of the optimization problems (6) and (11), respectively for the following cases: i) $1 < \alpha < \infty$, ii) $\alpha = \infty$, iii) $\alpha = 1$, and iv) $\alpha < 1$ of eqs. (1), (2). For illustration, fig. 1 shows the solutions for the optimization problem for a PRC for the Hodgkin-Huxley neuron model along with the escort functions of probability distributions maximizing the Tsallis entropy. Here, mathematical details related to obtaining solutions with Hölder's inequality are omitted, as they are presented in [10,11].

i) Case for $1 < \alpha < \infty$: The optimal forcing $f_{\mathrm{opt},\, r}$ is obtained by setting $\alpha = r$ in the equality condition of eq. (1),

$$f_{\mathrm{opt},\, r}(\theta) = M \mathrm{sgn}[g(\theta)] (|g(\theta)| / \|g\|_{\frac{r}{r-1}})^{\frac{1}{r-1}}, \tag{12}$$

where g is given as in eq. (5) and this representation is proved to be unique, *i.e.*, there is no other optimal forcing without that in eq. (12) [10]. The two parameters $\Delta\phi$ and μ in $g(\theta)$ of eq. (5) are determined by solving two nonlinear equations of $\Delta\phi$ and μ, which are obtained by plugging eq. (12) into the constraints $\langle f \rangle = 0$ and $\|f\|_r = M$ [10,11]. This solution (12) results in a relatively smooth forcing signal; the shape of the signal often resembles that of the PRC as far as r takes a moderate value. As a special case, the power-reduced forcing (in fig. 1(c)) is obtained from eq. (12) for $r = 2$.

Similarly to the optimal forcing $f_{\mathrm{opt},\, r}$, the optimal PDF to Tsallis entropy (7) is obtained by setting $\alpha = q^{-1}$ (*i.e.*, $0 < q < 1$) in the equality condition of eq. (1),

$$p_{\mathrm{opt},\, q}(x) = \gamma^{\frac{1}{q}} |\lambda h(x) + (1-\lambda)\sigma^2|^{\frac{1}{1-q}}, \tag{13}$$

where γ and λ are determined from the constraints in eq. (8) and a cut-off is naturally introduced, *i.e.*, $p_q(x) \equiv 0$ for x satisfying $\lambda h(x) + (1-\lambda)\sigma^2 < 0$. As a result,

$$p_{\mathrm{opt},\, q}(x) = \frac{1}{Z_q} \left[1 - \frac{1-q}{3-q} \frac{x^2}{\sigma^2} \right]_+^{\frac{1}{1-q}} \tag{14}$$

in [13,14] is recovered, where $Z_q = (\frac{3-q}{1-q}\sigma^2)^{\frac{1}{2}} B(\frac{2-q}{1-q}, \frac{1}{2})$ and $[a]_+ \equiv \max(a, 0)$.

ii) Case for $\alpha = \infty$: Similarly to the case of $1 < \alpha < \infty$, Hölder's inequality (1) results in the optimal forcing by setting $\alpha = r = \infty$,

$$f_{\mathrm{opt},\, \infty}(\theta) = M \mathrm{sgn}[g(\theta)], \tag{15}$$

which is consistent with the limit of eq. (12) as $r \to \infty$ and its uniqueness is proved [10]. $\Delta\phi$ and λ in $g(\theta)$ of eq. (15) are determined, similarly to the above case for $1 < \alpha < \infty$. Note that this forcing shown in fig. 1(e) corresponds to the bang-bang control obtained under the magnitude-reduced constraint [15].

As for Tsallis entropy, $\alpha = \infty$ (*i.e.*, $q = \alpha^{-1} = 0$) implies $p(x)^q \equiv 1$ for $p(x) > 0$ in eq. (7). Hence, Tsallis entropy is maximized for any $p(x)$ with the compact support $[-\sqrt{3}\sigma, \sqrt{3}\sigma]$ although a detailed argument for this is omitted here. Also from eq. (13) it is proved that the escort function of $p_{\mathrm{opt},\,q}(x)$ converges to the step function $P_{\mathrm{opt},\,0}(x)$ shown in fig. 1(h) (pointwise, $q \to 0+0$).

iii) Case for $\alpha = 1$: In contrast to the case ii), from eq. (1) with $\alpha = 1$, $f_{\mathrm{opt},\,1}$ is proved to become a pair consisting of one arbitrarily tall negative pulse and one arbitrarily tall positive pulse (*i.e.*, bipolar pulses) separated by $\Delta\phi_{\max}$ [10] as shown in fig. 1(d). Since this optimal forcing for $r = 1$ includes only one parameter $\Delta\phi_{\max}$, the optimal $\Delta\phi_{\max}$ is determined algorithmically from Z, simply by tuning $\Delta\phi_{\max}$ in the range of $[0, \pi]$ and observing the resulting locking range $L[f]$ for each $\Delta\phi_{\max}$ numerically or experimentally.

In contrast to the case of $q = 0$, Tsallis entropy (7) is not defined at $q = 1$. However, it is known that it converges to the Gaussian distribution as $q \to 1 + 0$ [13].

iv) Case for $\alpha < 1$: As opposed to the above cases of $1 \leq r\ (= \alpha) \leq \infty$, it is not known that $f_{\mathrm{opt},\,r}$ has any physical interpretation for $r < 1$. However, for Tsallis entropy, the case of $q = \alpha^{-1} > 1$ is important from its applications, since it captures the power-law distributions with heavy tails. Similarly to the case of $0 < q < 1$, the optimal PDF $p_{\mathrm{opt},\,q}(x)$ is uniquely obtained as the same formula in eq. (14), by setting $\alpha = q^{-1}$ (*i.e.*, $q > 1$) in the equality condition of eq. (2). Note that Z_q is obtained as $Z_q = (\frac{3-q}{q-1}\sigma^2)^{\frac{1}{2}} B(\frac{3-q}{2(q-1)}, \frac{1}{2})$ and $q < 3$ is naturally required.

Simulations. – The principal predictions of the theory are first confirmed in numerical simulations of a chemical corrosion model (see [19]) describing the electrodissolution of nickel in sulfuric acid. The dimensionless model simulates the variation of the electrode potential E and surface coverage Θ of oxide species with time t at a constant circuit potential V and cell resistance S,

$$\frac{\mathrm{d}E}{\mathrm{d}t} = \frac{V-E}{S} - \left[\frac{c_h \exp(E/2)}{1 + c_h \exp(E)} + a\exp(E)\right](1-\Theta),$$
$$G\frac{\mathrm{d}\Theta}{\mathrm{d}t} = \frac{\exp(E/2)}{1 + c_h \exp(E)}(1-\Theta) - \frac{b\ c_h \exp(2E)}{c\ c_h + \exp(E)}\Theta. \quad (16)$$

The model parameters were chosen to produce limit cycle oscillations close to a supercritical Hopf bifurcation, namely, the dimensionless circuit potential V is set at 15, acid concentration c_h is set at 1600, and kinetic parameters are $a = 0.3$, $b = 6 \times 10^{-5}$, $c = 0.001$, $S = 20$, and $G = 0.01$. The PRF Z for perturbation of the electrode potential is shown in fig. 2(a). The PRF was applied to obtain three optimal waveforms for the power-, magnitude-, and area-reduced constraints as shown in fig. 2(b). For power-constraint, the waveform coincides with the generic optimal waveform $Z(\theta+\pi) - Z(\theta)$ [1], and has a relatively smooth character that retains the odd harmonic components of the PRC. The waveforms for the magnitude- and area-constraint are also the simplest ones expected for 50% duty cycle square wave and two evenly paced bipolar pulses, respectively. The relatively simple shapes of the optimal waveforms imply that under these conditions the oscillations have relatively weak nonlinear characters.

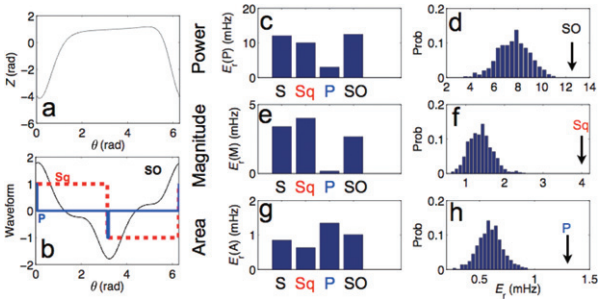

Fig. 2: (Color online) Simulation results from optimal synchronization of a chemical oscillatory model (16). (a) PRF. (b) Three waveforms: Sq: square wave (thick dashed line). P: pulse wave (thick solid line). SO: smooth (power-reduced) optimal waveform determined as $Z(\theta+\pi) - Z(\theta)$. (c), (e), (g): synchronizabilities $E_r(P)$, $E_r(M)$, $E_r(A)$ for power-, magnitude-, and area-reduced constraint, respectively. For comparison, results of sinusoidal synchronization simulations are also shown (waveform S). (d), (f), (h): synchronizability histogram for 1000 random waveforms for power-, magnitude-, and area-reduced constraint, respectively. The random waveforms were generated with uniformly distributed random numbers for the Fourier coefficients of the waveforms up to five harmonics. The arrow denotes the maximum synchronizability limit obtained by smooth optimal $f_{\mathrm{opt},\,2}$, square $f_{\mathrm{opt},\,\infty}$, and pulse $f_{\mathrm{opt},\,1}$, respectively.

To compare the synchronizing capability of different waveforms, we defined the reduced synchronizabilities E_r as follows. Numerical simulations for the synchronization of the oscillations were carried out by periodically varying the circuit potential variable as $V = 15 + Af(\Omega t)$. The simulations were conducted at fixed forcing frequencies Ω and the amplitude A of the waveform was increased until synchronization occurs where the critical amplitude A_c was recorded. The reduced synchronizabilities E_r are defined as

$$E_r = |\Delta\omega|/A_c R, \quad (17)$$

where R is the rescaling factor that enables a comparison of different signals for their power ($R = \|f\|_2 = \langle f^2\rangle^{\frac{1}{2}}$), magnitude ($R = \|f\|_\infty = \text{ess. sup.}\,(|f|)$), or area ($R = \|f\|_1 = \langle|f|\rangle$). The average value of the reduced synchronizability for fixed positive and negative detunings is proportional to the width of the Arnold tongue at a given value of the constraint; therefore, it is a useful quantity to characterize the synchronizing capability of a waveform. In the following, 2% detuning was applied, namely $\Delta\omega/\omega = \pm 0.02$.

The simulations confirmed that for power-, magnitude-, and area-reduced synchronizabilities the smooth optimal, square, and pulse waveforms generate the widest locking range $L[f]$ (see figs. 2(c), (e), and (g); for comparison,

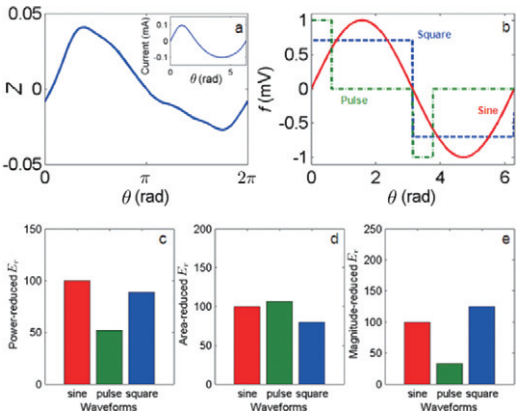

Fig. 3: (Color online) Experimental results from optimal synchronization control of oscillations close to Hopf bifurcation ($V_s = 1.080\,\mathrm{V}$) with three chosen waveforms. (a) The experimentally measured nearly harmonic PRF of the oscillations and the shape of oscillations (inset). (b) The three considered control waveforms: sine (red), pulse (green) and square (blue). (c), (d), (e): comparison of the reduced synchronizability $E_r(P), E_r(A), E_r(M)$ for three constraints: power-, area-, and magnitude-reduced constraint, respectively. The entrainabilities are linearly renormalized such that the value for the sinusoidal waveform is 100. The same colors are used for waveforms as in panel (b).

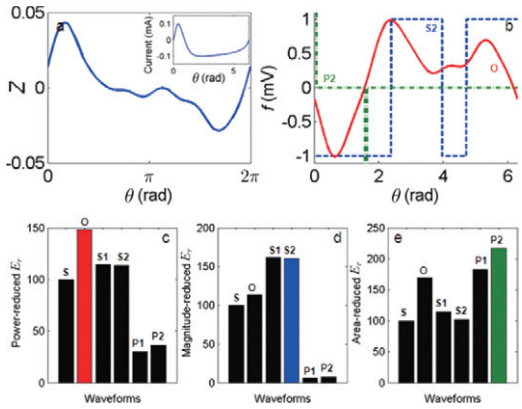

Fig. 4: (Color online) Optimal synchronization control of experimental relaxation oscillations far away from Hopf bifurcation ($V_s = 1.180\,\mathrm{V}$). (a) The experimentally measured PRF and the waveform (inset). (b) The three optimal control waveforms corresponding to the three examples: optimal wave (red) for power, optimal thin pulse (green, pulse width: $0.011T$) for area, and double square (blue) for magnitude constraints. (c), (d), (e): comparison of the reduced synchronizability (E_r) for all the six controls in three constraints: power-, area-, and magnitude-reduced constraint, respectively. The entrainabilities are linearly renormalized such that the value for the sinusoidal waveform is always 100. The same colors are used for waveforms as in (b), with other waveforms in black. (Symbols: S for sine, O for power optimal, S1 for $0.5T$-separated square shown in fig. 3(b), S2 for optimal double square, P1 for $0.5T$-separated thin pulse, P2 for optimal thin pulse).

results for synchronization with sinusoidal waveform are also presented). As a further confirmation of the nontrivial shapes of the optimal waveforms, we also performed corresponding numerical simulations with 1000 waveforms with random Fourier coefficients. The histogram of the synchronizabilities (see figs. 2(d), (f), and (h)), show that these random waveforms have bell-shape distributions whose range is below the synchronizability limited by the corresponding optimal waveform.

Experiments. – The enhancement of synchronization with optimized forcing waveforms was verified in experiments with an electrochemical oscillating reaction. The experimental system was a standard three-electrode electrochemical cell (controlled with a Gamry Reference 600 potentiostat) with a 1 mm diameter Ni-wire working electrode in 3 M sulfuric acid electrolyte, a 1.5 mm Pt-coated Ti-rod counterelectrode, and a $Hg/Hg_2SO_4/K_2SO_4$ (sat) reference electrode. (All potentials are given with respect to the reference electrode.) The cell was kept at a temperature of 10 °C. When a certain fixed circuit potential $V = V_s$ is applied with a 1 kOhm external resistance attached in series with the Ni wire, oscillatory behavior can be observed that occurs through a Hopf bifurcation at $V_s = 1.06\,\mathrm{V}$ with the period $T \sim 2.2\,\mathrm{s}$. The forcing signal waveform $f(\Omega t)$ $(= f(\theta))$ is superimposed on the circuit potential such that $V = V_s + Af(\theta)$, where A is the amplitude. The output signals were collected and analyzed using a National Instruments Labview data acquisition system at 100 Hz and 1000 Hz sample acquisition rate for the synchronization experiments and PRF measurements, respectively. The phase of the oscillations was determined with the Hilbert transform method [18].

At a fixed circuit potential $V_s = 1.080\,\mathrm{V}$, the system is close to Hopf bifurcation and the oscillation waveform and the phase response function are nearly harmonic as shown in fig. 3(a). For such nearly harmonic waveform PRFs, the optimal waveforms are smooth sinusoidal, two evenly paced pulses, or a 50% duty cycle square wave for the power-, area-, and magnitude-reduced constraint, respectively. (Here, the pulse wave has a width of $0.1T$.) We measured reduced synchronizabilities E_r of these three waveforms at each constraint, and compared them separately (figs. 3(c), (d) and (e)). As predicted by the theory, the smooth sinusoidal, pulse, and square waves are superior to the others for power-, area-, or magnitude-reduced constraint, respectively. Even for this relatively harmonic PRF, the optimal wave can outperform the others by 6% to 93% depending on the specific constraint and waveform.

The chemical oscillation waveform and PRF include strong higher harmonics when the electrodes are polarized at an elevated potentials of $V_s = 1.180\,\mathrm{V}$ as shown in fig. 4(a). For this system, we also used the theory to determine the optimal waveforms for the three constraints as shown in fig. 4(b). For the minimum-power constraint, the optimal waveform is a smooth signal whose shape is connected to that of the PRF in a highly nontrivial manner. For the area constraint, the two pulses are separated by a

nontrivial time of $0.25T$ instead of the usual $0.5T$ for the harmonic case. For the magnitude constraint, the optimal square waveform has a double-square shape; each square shape has a different size and the two square waves are separated by $0.38T$. We measured the synchronizability for the three optimal waves as well as those obtained for the harmonic PRFs. This comparison is expected to reveal the importance of higher harmonics in the PRF for the experimental system. The experimental result for the power constraint (fig. 4(c)) shows that the optimal smooth waveform clearly outperforms the other tested waveforms; for example, the synchronizability is enhanced by 50% compared to the smooth sinusoidual waveform. For the area-reduced constraint (fig. 4(e)) the situation is similar; the optimal pulse waveform is 19% better than the $0.5T$ separated pulse, and over two times better than a simple sine wave. These results imply that the sinusoidal waveform can be very poor for the power- and area-reduced constraint cases. Finally, for the magnitude-reduced forcing (fig. 4(d)), the optimal wave achieves about the same performance as a 50% duty cycle square wave does. However, in this example we can still see some effect of higher harmonics; the difference between the square wave and the sine wave is greatly enhanced (60%) in contrast to the relatively smaller enhancement (25%) observed with the nearly harmonic PRF.

Conclusion. – We showed that the optimal synchronization problem can be translated into Tsallis entropy maximization, which can be solved by Hölder's inequality. This mathematical finding provides an important physical realization of the widely known and commonly used inequality. The numerical and experimental results in a chemical system confirmed the efficiency of Tsallis entropy maximization analogy design of forcing waveforms for optimal synchronization. Because the theory in the present paper is independent of the details of a system, it could also apply to other optimal designs such as those in practical electrical circuits [20], in micro- and nano-integrated circuit oscillators [8] as well as in biology for PRF-based synchronization of neuronal spiking or circadian rhythm. Further theoretical treatment is required for noisy environment, oscillator networks, or for strongly forced oscillators [21]; such attempts could be possible with the development of the phase model theory.

* * *

This work was supported by MEXT (No. 26286086) and by the Telecommunications Advancement Foundation in Japan. IZK acknowledges support from National Science Foundation CHE-0955555 grant. The authors are grateful to Prof. Constantino Tsallis for fruitful discussions and to Prof. Hiroki Suyari for his critical reading of our manuscript. The authors would also like to thank the reviewers for providing valuable comments.

REFERENCES

[1] Harada T., Tanaka H.-A., Hankins M. J. and Kiss I. Z., *Phys. Rev. Lett.*, **105** (2010) 088301.
[2] Zlotnik A., Chen Y., Kiss I. Z., Tanaka H.-A. and Li J. S., *Phys. Rev. Lett.*, **111** (2013) 024102.
[3] Bagheri N., Stelling J. and Doyle F. J., *PLoS Comput. Biol.*, **4** (2008) e1000104.
[4] Aihara K., Matsumoto G. and Ikegaya Y., *J. Theor. Biol.*, **109** (1984) 249.
[5] Jackson J. C., Windmill J. F. C., Pook V. G. and Robert D., *Proc. Natl. Acad. Sci. U.S.A.*, **106** (2009) 10177.
[6] Fukuda H., Murase H. and Tokuda I. T., *Sci. Rep.*, **3** (2013) 1533.
[7] Luther S. *et al.*, *Nature*, **475** (2011) 235.
[8] Takano K., Motoyoshi M. and Fujishima M., *Proceedings of the IEEE Asian Solid-State Circuits Conference, Korea., 2007* (IEEE) 2007, p. 336.
[9] Wilson D. and Moehlis J., *SIAM J. Appl. Dyn. Syst.*, **13** (2014) 276.
[10] Tanaka H.-A., *Physica D: Nonlinear Phenom.*, **288** (2014) 1.
[11] Tanaka H.-A., *J. Phys. A: Math. Theor.*, **47** (2014) 402002.
[12] Hardy G., Littlewood J. E. and Pólya G., *Inequalities*, second edition (Cambridge Mathematical Library) 1988.
[13] Tsallis C., *Introduction to Nonextensive Statistical Mechanics* (Springer, New York) 2009.
[14] Prato D. and Tsallis C., *Phys. Rev. E*, **60** (1999) 2398.
[15] Nabi A. and Moehlis J., *J. Math. Biol.*, **64** (2012) 981.
[16] Kuramoto Y., *Chemical Oscillations, Waves and Turbulence* (Springer, Berlin) 1984.
[17] Winfree A. T., *The Geometry of Biological Time*, 2nd edition (Springer, New York) 2001.
[18] Pikovsky A. S., Rosenblum M. G. and Kurths J., *Synchronization: A Universal Concept in Nonlinear Sciences* (Cambridge University Press, Cambridge) 2001.
[19] Pyragas K., Pyragas V., Kiss I. Z. and Hudson J. L., *Phys. Rev. Lett.*, **89** (2002) 244103.
[20] Nagashima T., Wei X., Tanaka H.-A. and Sekiya H., *IEEE Trans. Circuits Syst.*, **61** (2014) 2904.
[21] Kurebayashi W., Shirasaka S. and Nakao H., *Phys. Rev. Lett.*, **111** (2013) 214101.